


# Salinomycin-Loaded High-Density Lipoprotein Exerts Promising Anti-Ovarian Cancer Effects by Inhibiting Epithelial–Mesenchymal Transition

Miao Zou, Xirui Yin, Xuan Zhou, Xinhui Niu, Yi Wang , Manman Su

Department of Regenerative Medicine, School of Pharmaceutical Sciences, Jilin University, ChangChun, People's Republic of China

Correspondence: Manman Su; Yi Wang, Department of Regenerative Medicine, School of Pharmaceutical Sciences, Jilin University, 1266 Fujin Road, Changchun, 130021, People's Republic of China, Tel/Fax +86 431 85619252, Email [summ@jlu.edu.cn](mailto:summ@jlu.edu.cn); [wangyi@jlu.edu.cn](mailto:wangyi@jlu.edu.cn)

**Background:** Effective treatments for ovarian cancer remain elusive, and survival rates have long been considered grim. Ovarian cancer stem cells (OCSCs) and epithelial–mesenchymal transition (EMT) are associated with cancer progression and metastasis, as well as drug resistance and eventual treatment failure. Salinomycin (Sal) has an extensive effect on a variety of cancer stem cells (CSCs); however, its poor water solubility and toxicity to healthy tissues at high doses limit further research into its potential as an anti-cancer drug. We proposed a therapeutic strategy by constructing a tumor-targeting carrier that mimics high-density lipoprotein (HDL) to synthesize salinomycin-loaded high-density lipoprotein (S-HDL). This strategy helps reduce the side effects of salinomycin, thereby improving its clinical benefits.

**Methods:** OCSCs were isolated from ovarian cancer cells (OCCs) and the uptake of HDL nanoparticles was observed using laser confocal microscopes. After the cell viability analysis revealed the inhibitory effect of S-HDL on OCCs and OCSCs, the main biological processes influenced by S-HDL were predicted with a transcriptome sequencing analysis and verified in vitro and in vivo.

**Results:** Cellular uptake analysis showed that the HDL delivery system was able to significantly enhance the uptake of Sal by OCCs, tentatively validating the targeting role of recombinant HDL, so that S-HDL could reduce the toxicity of Sal and increase its anti-ovarian cancer effects. Conversely, S-HDL could exert anti-ovarian cancer effects by inhibiting the proliferation of OCCs and OCSCs, promoting apoptosis, blocking EMT, and suppressing stemness and angiogenesis-related protein expression in vitro and in vivo.

**Conclusion:** S-HDL had stronger anti-ovarian cancer effects than unencapsulated Sal. Thus, it may be a potential agent for ovarian cancer treatment in the future.

**Keywords:** ovarian cancer, ovarian cancer stem cells, epithelial–mesenchymal transition, salinomycin, high-density lipoprotein

## Introduction

Ovarian cancer (OC) is a gynecological disease, with as little as 30% of its patients surviving five years.<sup>1,2</sup> Tumor heterogeneity, a hallmark of malignancy, is mainly induced by the plasticity of cancer stem cells (CSCs) and epithelial–mesenchymal transition (EMT), which leads to treatment resistance and influences disease progression.<sup>3</sup> CSCs constitute a small subpopulation of cancer cells that possess stemness, strong tumorigenic potential, unlimited self-renewal ability, multidirectional differentiation, metastasis, and treatment resistance. Most standard treatments eliminate relatively differentiated and proliferating tumor cells, leaving mostly dormant CSCs, subsequently leading to tumor recurrence and metastasis.<sup>4,5</sup>

CSCs can also drive invasion and metastasis by inducing EMT, which, in turn, fosters migration and recolonization of cancer cells within metastatic niches.<sup>6</sup> During the EMT process, cancer cells gain stemness and motility,<sup>7,8</sup> leading to migration and metastasis. Therefore, the development of drugs that can effectively eliminate all CSCs and inhibit EMT, is crucial for the treatment of OC.

Salinomycin (Sal), a selective membrane ionophore antibiotic<sup>9</sup> that has extensive effects on a variety of CSCs,<sup>10–13</sup> including induction of apoptosis, autophagy, oxidative stress, and inhibition of tumor cell proliferation, angiogenesis and stemness.<sup>14–17</sup> Sal can also inhibit tumor invasion and migration by targeting the Wnt and EMT pathways.<sup>18,19</sup> Sal has significant therapeutic potential as an anti-cancer agent. However, it has poor water solubility, and, at high doses, it is toxic to healthy tissues. Consequently, researching Sal as an anti-cancer drug is challenging.<sup>20,21</sup>

Bionic targeting drug delivery systems increase anti-cancer drug accumulation in tumors by facilitating cellular uptake and intracellular retention, and reducing the drug's toxicity to non-cancerous tissues.<sup>22</sup> A high-density lipoprotein (HDL), which carries lipids as multifunctional aggregates in the plasma, can be used as an effective carrier for hydrophobic drugs because of its phospholipid core.

Here, we proposed a therapeutic strategy to construct tumor-targeting carriers by mimicking HDL and synthesized salinomycin-loaded high-density lipoprotein (S-HDL) by the sodium cholate method. Apolipoprotein A-I (ApoA-I), a major component of the S-HDL shell, exerts anti-tumor effects in concert with Sal.<sup>23</sup> Apolipoprotein E (ApoE) binds to low-density lipoprotein receptor-related protein 1 (LRP-1),<sup>24</sup> which is highly expressed in OC tissues. Therefore, S-HDL can target OC tissues and exert an efficient anti-tumor effect, while reducing the toxic effects on healthy tissues.

In this study, we synthesized S-HDL, using recombinant human ApoA-I (rhApoA-I) and recombinant human ApoE (rhApoE) as the shell and Sal as its hydrophobic core. Ovarian cancer stem cells (OCSCs) were isolated from ovarian cancer cells (OCCs) and the efficacy of S-HDL on both these cell types, was analyzed with a cell viability assay. Furthermore, the biological processes by which S-HDL affects OCCs were examined with a transcriptome sequencing analysis. The anti-cancer effects of S-HDL, were verified *in vitro* and *in vivo*.

## Materials and Methods

### Materials

Human ovarian cancer cells (SKOV3 cells) and human ovarian epithelial cells (IOSE80 cells) were purchased from the Cell Bank of the Chinese Academy of Sciences. RhApoA-I and rhApoE were prepared and stored in our laboratory. Sal was purchased from Selleck Co., Ltd. (China). Rabbit antibodies against c-Myc, Sox-2, Nanog, Oct-4, E-cadherin, vimentin, N-cadherin,  $\beta$ -catenin, and cleaved caspase-3 were obtained from Cell Signaling Technology (USA). Rabbit antibodies against LRP-1, Bax, and Bcl-2 were purchased from Abcam (Cambridge, USA). The Annexin V-FITC/PI apoptosis detection kit and PE-conjugated anti-human CD133 antibody were purchased from BD Biosciences (USA). The biotin-conjugated anti-human CD133 antibody was purchased from Miltenyi Biotec (Germany). The CELLlection Biotin Binder Kit was purchased from Invitrogen (USA). The basic fibroblast growth factor (bFGF) and epidermal growth factor (EGF) were bought from Peprotech (USA). The B27 supplement was obtained from Gibco (USA). The DMEM and DMEM/F12 medium, RIPA 1640, and Fetal Bovine Serum (FBS) were purchased from Biological Industries (Israel). Lecithin and coumarin 6 (C6) were purchased from Sigma-Aldrich (USA). Protease inhibitors were obtained from Thermo Fisher Scientific (USA). Horseradish Peroxidase-conjugated secondary antibody was bought from Absin Bioscience Co., Ltd. (China).

### Synthesis of S-HDL

S-HDL was synthesized with Sal, rhApoA-I, rhApoE, and lecithin, using the sodium cholate method, as we previously described.<sup>25</sup> Briefly, an ethanol solution (1 mL), containing 2.7 mg lecithin and 1 mg Sal, was rapidly injected into 6 mL of PBS (pH = 7.4). After adding N<sub>2</sub>, 0.75 mL PBS, containing 2.7 mg sodium cholate, 5 mg rhApoA-I and 2.5 mg rhApoE, was added to the lipid mixture by stirring. After being incubated at room temperature for 30 min and then at 4°C for 12 h, the solution was dialyzed against PBS at 4°C, to completely remove ethanol and sodium cholate. The S-HDL concentration was calculated based on the encapsulated Sal content.

### Cell Culture, OCSCs Isolation and Identification

IOSE80 and SKOV3 cells were cultured in DMEM and RIPA1640, respectively, both mediums supplemented with 10% FBS, at 37°C in 5% CO<sub>2</sub> humidified atmosphere. The OCSCs subpopulations were isolated from SKOV3 cells by

immunomagnetic bead sorting. Briefly, OCCs were collected and incubated with biotin conjugated anti-human CD133 antibody at 4°C for 10 min in the dark and then sorted, using a CELLection Biotin Binder kit. CD133<sup>+</sup> OCSCs were cultured in DMEM/F12 medium, supplemented with 20 ng/mL EGF, 20 ng/mL bFGF, and 1% B27, at 37°C in 5% CO<sub>2</sub>.

Based on the detection of cell-surface markers, flow cytometry identified the OCSCs. Both OCCs and OCSCs were incubated with the PE-conjugated anti-human CD133 antibody at 4°C for 20 min in the dark, and detected with a flow cytometer. Western blotting was conducted to analyze the expression of stemness markers such as c-Myc, Nanog, Sox-2, and Oct-4, to further characterize the OCSCs.

## Western Blotting Analysis

For OCSCs identification and LRP-1 expression analysis, the total cellular proteins were extracted from untreated OCCs and OCSCs. In pharmacodynamic experiments, total cellular proteins were extracted from OCCs, OCSCs, and xenograft tumors, all treated with different concentrations of S-HDL, and quantified. Equal amounts of protein samples (60 µg), mixed with loading buffer, were boiled for 10 min and loaded onto an SDS-PAGE gel. Thereafter, the proteins were transferred to PVDF membranes, blocked with 10% non-fat milk for 15 min, incubated with primary antibodies overnight at 4°C, and then incubated with the secondary antibody for 1 h. The protein bands were visualized using Immobilon Western Chemiluminescent HRP substrate.

## Expression of LRP-1 and Cellular Uptake of C6-Loaded HDL (C6-HDL)

The expression of LRP-1 in OCCs, OCSCs, and IOSE80 cells was analyzed by Western blotting, as described above. Subsequently, C6-HDL was synthesized by encapsulating the C6 fluorescent dye, instead of Sal, in the HDL shell and quantified, using a multifunctional microplate analyzer. As they were cultured in suspension, OCSCs were not eligible to undergo a cellular uptake analysis. OCCs and IOSE80 cells were treated with 300 ng/mL C6 or C6-HDL for 2 h, respectively, and the cellular uptake of C6 was observed by confocal laser microscopy (FITC, NIKON C2).

## Cell Proliferation Assay

OCCs and OCSCs (1×10<sup>4</sup> cells/well) were seeded in 96-well plates for 24 h, followed by treatment with different concentrations of S-HDL and Sal, for 48 h. The Cell Counting kit-8 (CCK8) was used to measure cell viability. The GraphPad Prism 8 was used to calculate the 50% inhibitory concentration (IC<sub>50</sub>).

## Transcriptome Sequencing Analysis

The gene expression profiles of OCCs, treated with 8 µg/mL S-HDL for 48 h, were obtained using transcriptome sequencing analysis. The *t*-test algorithm was selected to identify differentially expressed genes (DEGs), and the fold change threshold was set at log<sub>2</sub> (fold change) > log<sub>2</sub> (1.5) or log<sub>2</sub> (fold change) < -log<sub>2</sub> (1.5), with the *P*-value < 0.05. The gene expression profiles of OCCs were compared with those of the control group to evaluate the gene expression level variation between the groups. Finally, Gene Ontology (GO) enrichment analysis was used to biologically annotate the effects of S-HDL on OCCs, and Kyoto Encyclopedia of Genes and Genomes (KEGG) was utilized to analyze the effects of S-HDL on the EMT process, which is regulated by Wnt/β-catenin.

## Verification of the Biological Process of S-HDL Affecting OCSCs

Around 5×10<sup>5</sup> cells/well were cultured in 6-well plates at 37°C for 24 h and then treated with 0.5 µg/mL, 2 µg/mL, and 8 µg/mL S-HDL, and 8 µg/mL Sal and PBS, respectively, for 24 h. Then, the cells were washed and incubated with 3 µL Annexin V-FITC and 3 µL PI for 15 min, in the dark at room temperature and analyzed using flow cytometry (BD FACSCanto II). In addition, Western blotting analysis was performed to evaluate the effects of S-HDL on stemness, EMT, and apoptosis-related proteins.

## Efficacy of S-HDL on Mice Model of Ovarian Cancer

Forty BALB/c-nu nude female mice (4–5 weeks old) were purchased from Beijing HFK Bioscience Co., Ltd, and maintained in a laminar airflow cabinet, under a specific pathogen-free environment. The mice were treated according to

the National Guidelines for the Care and Use of Laboratory Animals. All animal protocols were approved by the Animal Ethics Committee of Jilin University.

After 1 week of acclimation,  $2 \times 10^6$  SKOV3 cells were subcutaneously injected into the left hind limb. After one week, tumor-bearing mice were randomly divided into six groups (six mice per group), to receive intravenous treatment with saline, S-HDL (l) (200  $\mu\text{g}/\text{kg}$  S-HDL), S-HDL (h) (400  $\mu\text{g}/\text{kg}$  S-HDL), S-HDL+DDP (200  $\mu\text{g}/\text{kg}$  S-HDL combined with 1 mg/kg cisplatin), DDP (2 mg/kg cisplatin), and Sal (400  $\mu\text{g}/\text{kg}$  Sal), once every three days for three weeks. The body mass of the mice was measured and noted every three days. After three weeks of treatment, the mice were euthanized and the tumors, serum, liver, and spleen were collected and weighed. To evaluate the anti-tumor mechanisms of S-HDL, the removed tumors were fixed in 4% paraformaldehyde for histological examination or frozen for Western blotting analysis.

## Tumor Histopathological Examination and Immunohistochemistry

The tumors were fixed, embedded, and stained with hematoxylin and eosin (H&E). The tumor sections were also incubated with the platelet-endothelial cell adhesion molecule (CD31), vascular endothelial growth factor (VEGF)-A, and hypoxia-inducible factor 1 alpha (HIF-1a) primary antibodies at 4°C overnight and then incubated at room temperature for 20 min with the secondary antibodies. After being stained with DAB and counterstained, all the slices were observed under a microscope.

## Evaluating the Hepatotoxicity and Cardiotoxicity

To evaluate the potential toxicity of S-HDL, the serum was harvested, and aspartate aminotransferase (AST), alanine transaminase (ALT), and creatine kinase (CK) levels were measured using commercial kits (Jiancheng Bioengineering Institute, China).

## Statistical Analysis

All statistical analysis were performed using GraphPad Prism 8.0. The Student's *t*-test was used to assess the statistical significance between the two experimental groups. Results are expressed as mean  $\pm$  SD. *P* values less than 0.05 were considered statistically significant.

## Results

### Isolation and Identification of OCSCs

The transmembrane glycoprotein, CD133, is the most common surface marker of hematopoietic and epithelial stem cells, and CSCs.<sup>26</sup> Immunomagnetic bead sorting isolated CD133<sup>+</sup> OCSCs, and identified by flow cytometer and Western blotting. The proportion of CD133<sup>+</sup> cells in OCSCs was 91.66%, considerably higher than the 6.06% in OCCs (Figure 1A), indicating that the CD133<sup>+</sup> subpopulation was successfully enriched in OCCs. Nanog, c-Myc, Oct-4, and

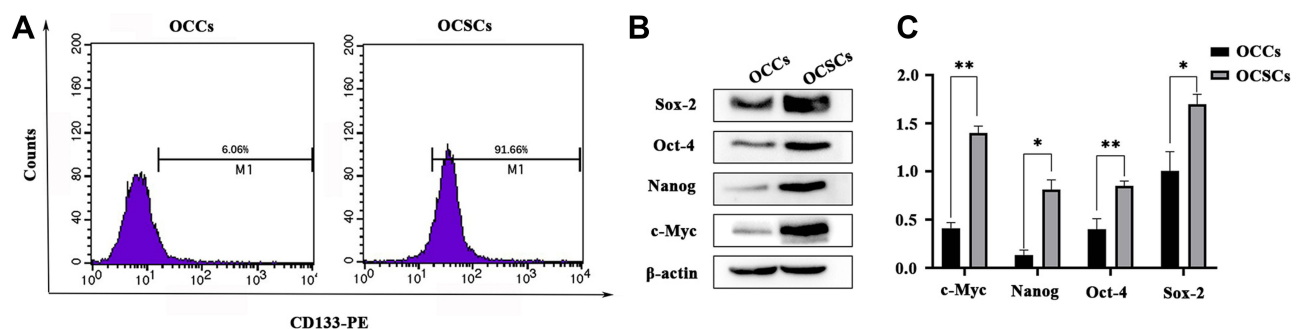


**Figure 1** Expression of CSCs markers on OCCs and OCSCs. **(A)** The expression of CD133 in OCCs and OCSCs assessed by flow cytometry. **(B)** The expression of c-Myc, Nanog, Oct-4 and Sox-2 (Western blotting analysis). **(C)** Relative protein level ( $\bar{x} \pm s$ ,  $n=3$ ) (\*\* $P < 0.05$ , \*\* $P < 0.01$ , \*compared with OCCs).

Sox-2 have been recognized as stemness markers. Compared to OCCs, the CD133<sup>+</sup> cells highly expressed Nanog, c-Myc, Oct-4, and Sox-2 (Figure 1B and C), further proving that CD133<sup>+</sup> cells had CSCs characteristics.

## Recombinant HDL Promoted Cellular Uptake of HDL Nanoparticles by OCCs

ApoE, a component of S-HDL, can specifically bind to LRP-1. Therefore, tumor cells with a high LRP-1 expression were more easily targeted by S-HDL. As shown in Figure 2A, the expression of LRP-1 in OCCs and OCSCs was significantly higher than that in IOSE80. Thus, S-HDL was more likely to be enriched in ovarian cancer tissues and reduced toxicity to normal tissues.

As shown in Figure 2B, OCCs showed weak uptake of free C6 and strong uptake of C6-HDL, indicating that recombinant HDL, as a carrier, could increase the uptake of C6 by OCCs. The uptake of HDL nanoparticles in different cells corresponded with the LRP-1 expression levels. The IOSE80 cells weakly expressed LRP-1, resulting in the uptake of fluorescent dyes. However, the proportion and fluorescent intensity of the C6-HDL taken up by the IOSE80 cells were lower than those of the OCCs. These results suggested that recombinant HDL had a targeting effect on OCCs, which might be related to the expression of LRP-1.

## S-HDL Exerted Stronger Cytotoxicity Than Unencapsulated Sal in OCCs and OCSCs

IC<sub>50</sub> represents the drug concentration required to reduce cell viability by 50% and is an important indicator for judging the efficacy of a drug. After treatment with different concentrations of S-HDL and Sal for 48 h, the cell viability of the OCCs and OCSCs was determined. As shown in Figure 2C, the cell viability of OCCs and OCSCs was dose-dependently inhibited by S-HDL, and the IC<sub>50</sub> of S-HDL on OCSCs was 2.937  $\mu\text{g}/\text{mL}$ , significantly lower than that of OCCs (28.04  $\mu\text{g}/\text{mL}$ ). Compared to the same concentration of Sal, S-HDL had a stronger inhibitory effect on OCCs and OCSCs (Figure 2D). Therefore, S-HDL exerted a stronger cytotoxicity than unencapsulated Sal in OCCs and OCSCs. The pre-

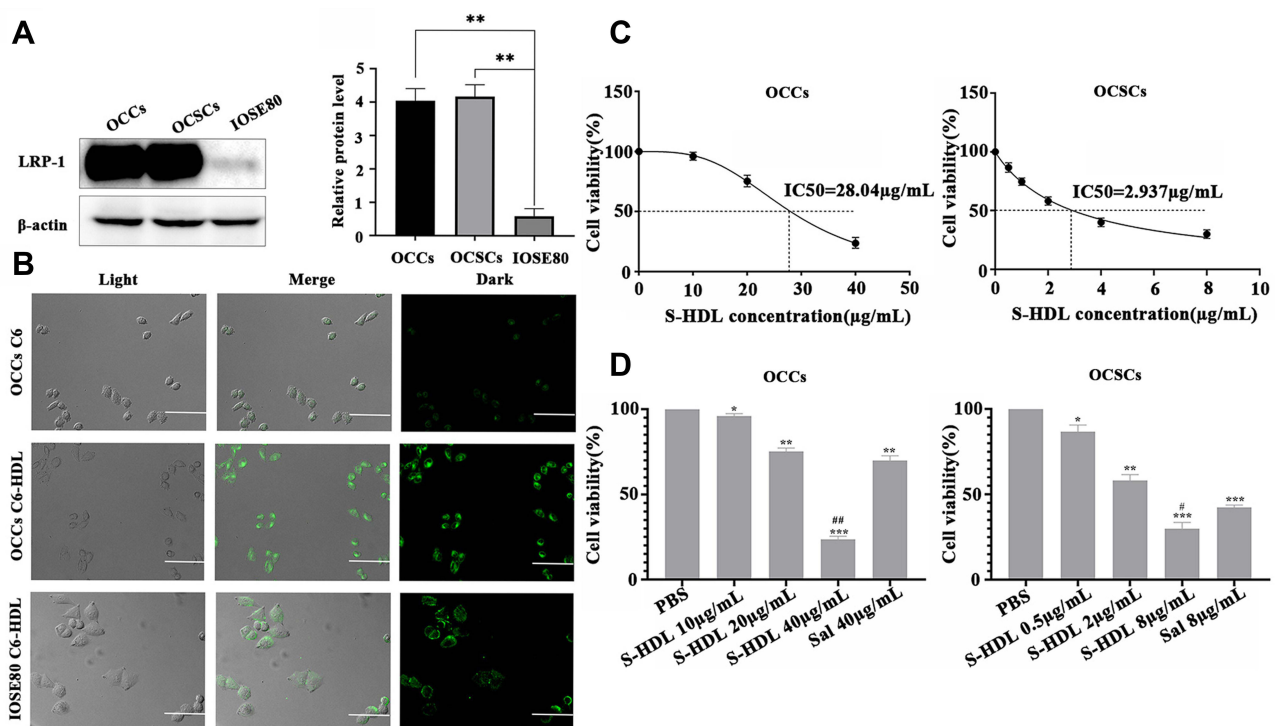


**Figure 2** Recombinant HDL promoted cellular uptake of HDL nanoparticles by OCCs and S-HDL exerted stronger cytotoxicity than unencapsulated Sal in OCCs and OCSCs. (A) Expression of LRP-1 in OCCs, OCSCs and IOSE80. (B) Cellular uptake of HDL nanoparticles (confocal laser microscope, scale bar = 50  $\mu\text{m}$ ) ( $\bar{x} \pm s$ , n=3) (\*\* $P < 0.01$ , compared with IOSE80 cells). (C) The IC<sub>50</sub> of S-HDL on OCCs and OCSCs for 48h treatment. (D) Cell viability of OCCs and OCSCs after being treated with different concentrations of S-HDL and Sal for 48h ( $\bar{x} \pm s$ , n=3) (\* $P < 0.05$ , \*\* $P < 0.01$ , \*\*\* $P < 0.001$ , \*compared with PBS treatment group, # $P < 0.05$ , ## $P < 0.01$ , ### $P < 0.001$ , compared with Sal treatment group).

test determined that a dose change in S-HDL between 0.5  $\mu\text{g/mL}$  and 8  $\mu\text{g/mL}$  significantly inhibited the OCSCs growth (13.3%–70.1% inhibition); the IC50 fell within this dose range. Therefore, concentrations of 0.5  $\mu\text{g/mL}$ , 2  $\mu\text{g/mL}$  and 8  $\mu\text{g/mL}$  S-HDL were selected for subsequent studies.

## Transcriptome Sequencing Analysis After S-HDL Treatment

OCCs treated with PBS and 8  $\mu\text{g/mL}$  S-HDL were used as the control and experimental group, respectively. To analyze the changes in gene expression related to S-HDL treatment, the *t*-test algorithm was used to screen DEGs, and GO enrichment was performed to reveal the biological processes that were affected by S-HDL. The results showed (Figure 3A) that DEGs were mainly related to biological processes, including cell migration, invasion, apoptosis, and immune responses. EMT is the main cause of tumor metastasis and invasion, and its occurrence is often regulated by the Wnt signaling pathway. Next, we performed a KEGG analysis and found that S-HDL suppressed the EMT process, mainly by upregulating tumor-suppressor genes, such as *DAB2*, *SMAD3*, *FOXA1*, *SFRP1*, and *DLG5*, and downregulating tumor-promoting genes, such as *CTNNB1*, *COL1A1*, *NKX2-1*, *EZH2*, and *S100A4*. As shown in Figure 3B, SMAD3, SFRP1, and  $\beta$ -catenin were involved in the Wnt/ $\beta$ -catenin pathway.  $\beta$ -catenin, encoded by *CTNNB1*, is the key protein in the Wnt signaling pathway, which facilitates the nuclear translocation and subsequent transcriptional activation of several genes involved in tumorigenesis and EMT.<sup>27</sup> Thus, we speculated that S-HDL could inhibit EMT by regulating  $\beta$ -catenin expression.

CSCs can drive invasion and metastasis by inducing EMT. When EMT is aberrantly activated in cancer cells, stemness is conferred to the cells and pathologically contributes to cancer progression. Therefore, the expression of stemness proteins in cancer cells is related to EMT and cancer progression.

We verified the effects of S-HDL on stemness, EMT, and apoptosis of OCSCs in the following experiments, according to the results of transcriptome sequencing analysis.

## S-HDL Inhibited Expression of Stemness Related Proteins in OCSCs

Stemness markers, such as c-Myc, Nanog, Oct-4, and Sox-2, remain active during the proliferation, migration, and invasion of malignant tumor cells and escape from the immune system, ultimately leading to chemotherapy resistance and recurrence of ovarian cancer. As shown in Figure 3C, OCSCs were treated with PBS, 0.5  $\mu\text{g/mL}$ , 2  $\mu\text{g/mL}$ , and 8  $\mu\text{g/mL}$  S-HDL and 8  $\mu\text{g/mL}$  Sal, respectively. S-HDL showed a strong dose-dependent inhibitory effect on the expression of the stemness markers in OCSCs.

## S-HDL Exerted Stronger Inhibiting Effects of EMT-Related Proteins in OCSCs

EMT is mainly manifested by the downregulation of the expression of epithelial cell markers, such as E-cadherin, and upregulation of the expression of mesenchymal cell markers, such as N-cadherin and vimentin.<sup>28,29</sup> Here, we observed that S-HDL dose-dependently suppressed the EMT process by increasing E-cadherin and decreasing the expression of N-cadherin, vimentin, and  $\beta$ -catenin (Figure 3D). Compared to the same concentration of Sal, S-HDL had a stronger inhibitory effect on EMT. These results suggested that S-HDL inhibiting the EMT process was related to the regulation of  $\beta$ -catenin, consistent with the results of transcriptome sequencing analysis.

## S-HDL Exerted Stronger Inducing Effects of Apoptosis in OCSCs

To investigate the efficacy of S-HDL on apoptosis in OCSCs, an Annexin-V/PI apoptosis assay and Western blotting analysis were performed. Compared to the same concentration of unencapsulated Sal, S-HDL elevated the apoptosis rate in OCSCs (Figure 4A and B). As shown in Figure 4C and D, S-HDL treatment also resulted in a significant dose-dependent increase in the expression of Bax and cleaved caspase-3 and inhibiting expression of Bcl-2. These results suggested that S-HDL exerted stronger inducing effects on apoptosis in OCSCs, consistent with the previous transcriptome sequencing analysis results.

## Efficacy of S-HDL on Human Ovarian Cancer Xenografted Mice

To evaluate the inhibitory effects of S-HDL on ovarian cancer, xenografted nude mice were allocated to a control, low- and high-dose experimental, and Sal control group, and treated with saline, 200  $\mu\text{g/kg}$  S-HDL, 400  $\mu\text{g/kg}$  S-HDL, and

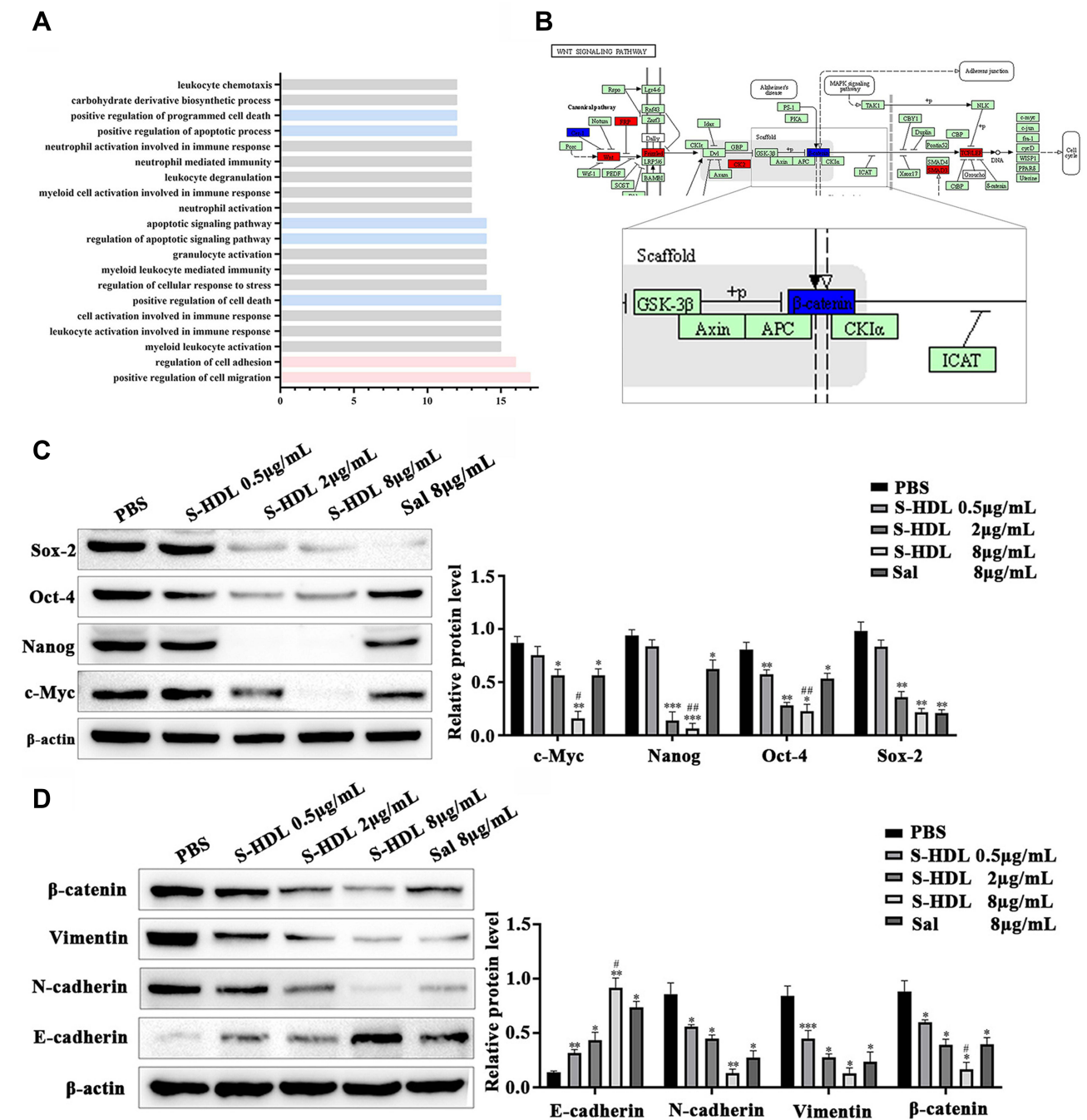


**Figure 3** Transcriptome sequencing analysis and verification. **(A)** Biological processes affected by S-HDL (GO enrichment analysis, red: migration and invasion related biological processes, blue: apoptosis related biological processes). **(B)** Effects of S-HDL on EMT process regulated by Wnt/ $\beta$ -catenin signal pathway (KEGG analysis). **(C)** Inhibitory effect on the expression of c-Myc, Nanog, Oct-4 and Sox-2 after treatment with PBS, S-HDL or Sal for 24h in OCSCs. **(D)** S-HDL depressed EMT process by increasing E-cadherin, and decreasing expression of N-cadherin, vimentin and  $\beta$ -catenin after treatment with PBS, S-HDL or Sal for 24h in OCSCs ( $\bar{x} \pm s$ , n=3) (\* $P < 0.05$ , \*\* $P < 0.01$ , \*\*\* $P < 0.001$ , \*compared with PBS treatment group; # $P < 0.05$ , ## $P < 0.01$ , ### $P < 0.001$ , #compared with Sal treatment group).

400  $\mu\text{g}/\text{kg}$  Sal, respectively. Cisplatin, the drug with the most extensive clinical application and substantial anti-tumor effect, was used as the positive control. After the xenografted nude mice were treated with saline, S-HDL (l), S-HDL (h), S-HDL+DDP, DDP, or Sal for 3 weeks, the tumors were removed. As shown in **Figure 5**, compared to the control group, the tumor size and weight, and the ratio of tumor weight to body mass were significantly reduced after treatment with S-HDL, S-HDL+DDP, DDP, and Sal. Notably, the inhibitory effects of S-HDL on ovarian cancer were stronger than

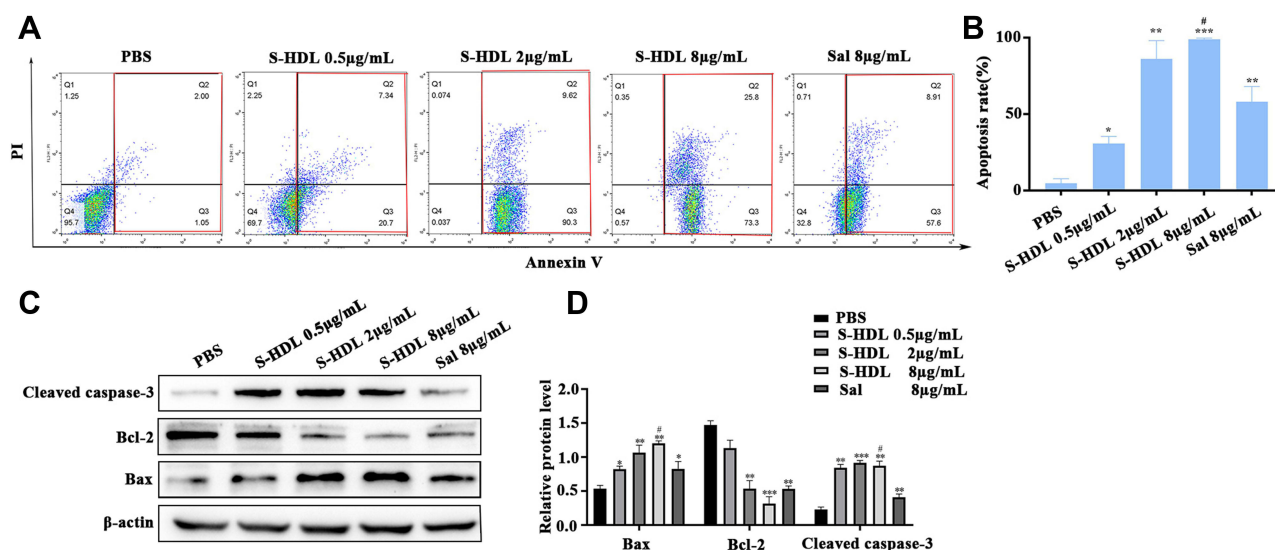


**Figure 4** S-HDL induced apoptosis in OCSCs. **(A)** Quadrant chart of cells distribution after treatment with PBS, S-HDL or Sal for 24h in OCSCs. **(B)** Bar graph representing apoptosis rate with different treatments in OCSCs. **(C)** Western blotting analysis results of the expression of Bax, Bcl-2 and cleaved caspase-3 after treatment with PBS, S-HDL or Sal for 24h in OCSCs. **(D)** The statistical value of relative protein level ( $\bar{x} \pm s$ ,  $n=3$ ) (\* $P < 0.05$ , \*\* $P < 0.01$ , \*\*\* $P < 0.001$ , \*compared with PBS treatment group; # $P < 0.05$ , #compared with Sal treatment group).

those of Sal at the same doses. It is speculated that recombinant HDL carriers could target and deliver encapsulated Sal to the tumor so that it could accumulate in the tumor, improving its inhibitory effects on ovarian cancer.

## Histological and Immunohistochemical Characterization

The histopathological examination (Figure 6A) showed extensive damage and neovascularization in the necrotic area, accompanied by numerous nuclear atypia and extensive lymphocytic infiltration in the tumors of saline treatment group. After treatment with 400 µg/kg S-HDL, the degree of inflammatory infiltration, neovascularization, and necrosis in the tumors decreased significantly.

VEGF, a major antiangiogenic therapy target for various types of malignant tumors, is induced by hypoxia through the HIF-1 $\alpha$ -dependent pathway<sup>30</sup> and plays an important role in tumor growth.<sup>31</sup> High levels of CD31 in vascular endothelial cells are intimately related to tumor angiogenesis.<sup>32</sup> As shown in Figure 6B–D, the different therapies significantly decreased expression of angiogenesis-related proteins VEGF-A, HIF-1 $\alpha$ , and CD31, compared to the control group. The positive expression rate of angiogenesis-related proteins in the S-HDL treatment group was lower than that of the Sal treatment group, at the same concentration. This indicated that S-HDL exerted stronger inhibitory effects on angiogenesis in xenograft tumors than unencapsulated Sal.

## Preliminary Study on the Safety of S-HDL

As shown in Figure 7A, the body mass of xenografted mice decreased in the S-HDL+DDP and DDP treatment groups after being removed tumor, while it remained almost unchanged in the S-HDL treatment and control group. Therefore, we hypothesized that S-HDL would have no or mild systemic toxicity.

The organ coefficients can preliminarily reflect the toxicity of the medicine. In our study, there was no significant difference in the liver and spleen coefficients in the S-HDL treatment group compared to the saline treatment group, while these coefficients were significantly decreased in the DDP treatment group. The liver coefficient of the Sal treatment group was particularly lowered (Figure 7B and C). This further suggested that S-HDL was less toxic than Sal.

As shown in Figure 7D–F, the levels of ALT, AST, and CK were significantly increased in the Sal treatment group compared with those in the saline treatment group, while S-HDL did not influence hepatic and myocardial function at the therapeutic dose used in our study.



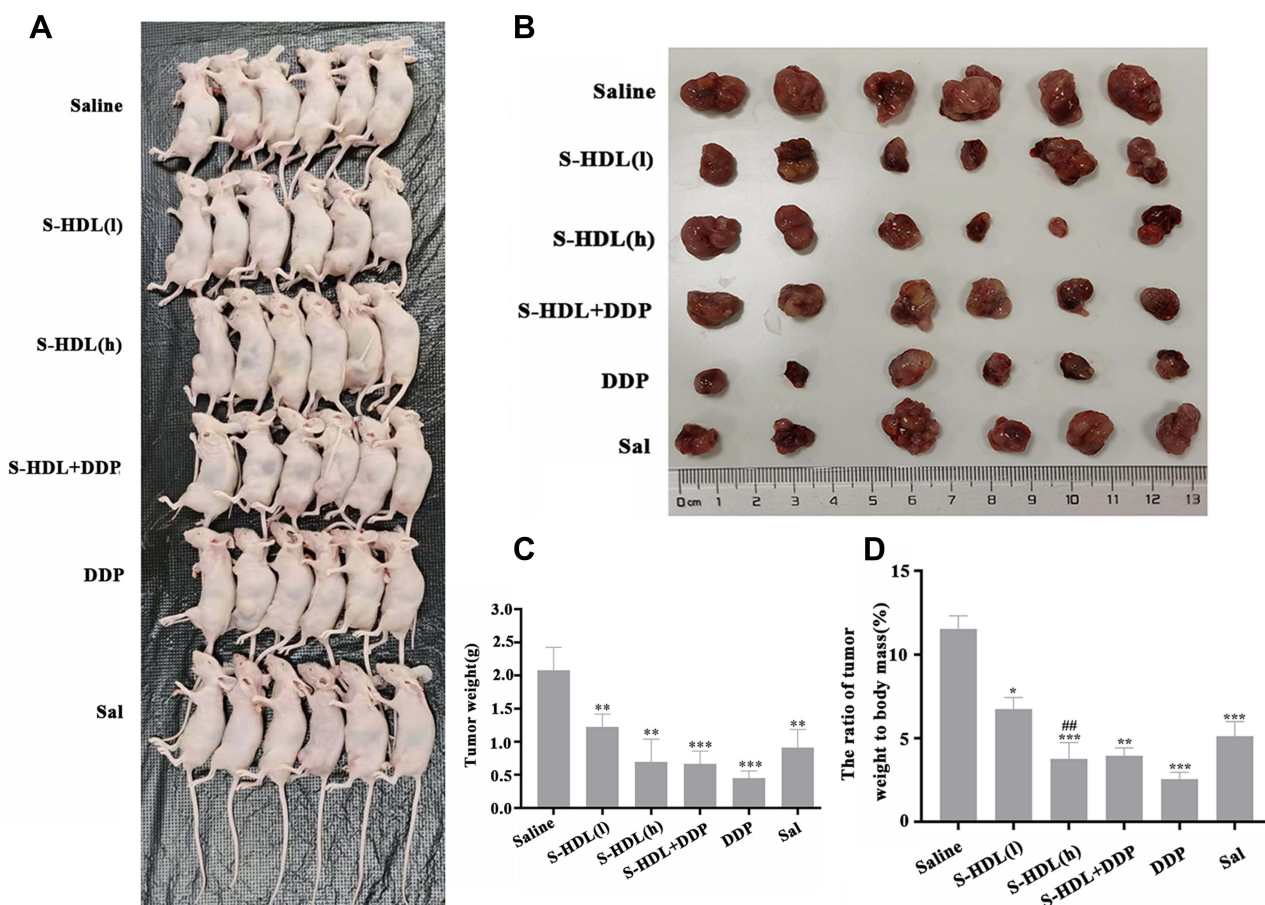


**Figure 5** Inhibitory effects of S-HDL on ovarian cancer xenografted mice. **(A)** Overall tumor formation in nude mice. **(B)** Tumor in xenografted mice after being treated with Saline, S-HDL (l) (200 $\mu$ g/kg S-HDL), S-HDL (h) (400 $\mu$ g/kg S-HDL), S-HDL+DDP (200 $\mu$ g/kg S-HDL combined with 1mg/kg cisplatin), DDP (2mg/kg cisplatin), and Sal (400 $\mu$ g/kg Sal) for 3 weeks. **(C)** Tumor weight of different groups. **(D)** The ratio of tumor weight to body mass ( $\bar{x} \pm s$ , n=6) (\* $P < 0.05$ , \*\* $P < 0.01$ , \*\*\* $P < 0.001$ , \*compared with Saline treatment group; ### $P < 0.01$ , #compared with Sal treatment group).

## S-HDL Blocked Stemness and EMT of Ovarian Cancer Cells in Xenografted Mice

The expression levels of multiple stemness markers (c-Myc, Nanog, Oct-4, and Sox-2) were significantly downregulated in response to S-HDL treatment. S-HDL also inhibited the EMT pathway by upregulating E-cadherin expression and downregulating the expression of N-cadherin, vimentin, and  $\beta$ -catenin in xenografted nude mice (Figure 8), which was consistent with previous results from OCCs.

## Discussion

Receptor-mediated targeting is a major approach for delivering hydrophobic drugs to tumors.<sup>22</sup> LRP-1, a multifunctional endocytic receptor that plays crucial roles in tumorigenesis and aggressiveness,<sup>33</sup> can specifically bind to ApoE. HDL has attracted widespread attention as a delivery carrier, owing to its unique characteristics. In this study, we demonstrated that recombinant HDL could increase the OCCs's uptake of encapsulated agentia, but not via the ovarian epithelial cells. Combined with the level of LRP-1 expression in different cell types, recombinant HDL may enhance the OCCs uptake of its encapsulated drugs, through specific binding to LRP-1.

Recombinant HDL also exhibits its own characteristics, including prolonged circulation time and accumulation in the tumor by the EPR effect.<sup>34</sup> In our study, S-HDL significantly enhanced the anti-tumor efficacy of Sal, both in vitro and in vivo. The results showed that, even at the same dose, S-HDL had a stronger anti-tumor effect than unencapsulated Sal. Therefore, to reduce the toxicity of Sal, a lower dose of Sal can be incorporated into S-HDL. Owing to the toxicity of the treatment drugs, chemotherapy patients are exposed to physical discomfort and significant health risks. Based on the fact

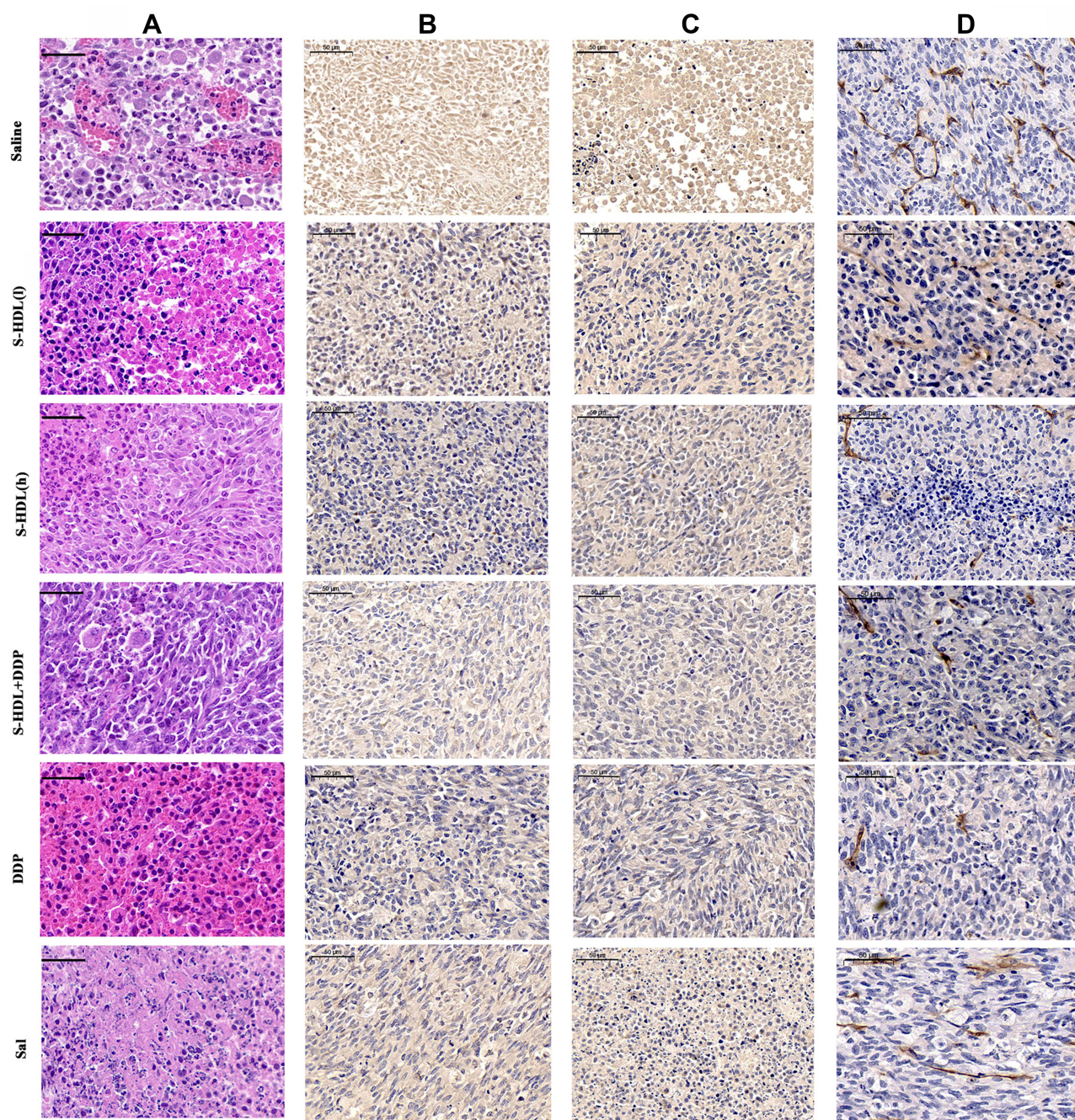


**Figure 6** Histological and immunohistochemical characterization. (A) HE staining results of ovarian cancer tissue in xenografted mice; S-HDL inhibited the expression of angiogenesis related proteins in ovarian cancer tissue (B) VEGF-A, (C) HIF-1 $\alpha$  and (D) CD31 (scale bar =50 $\mu$ m).

that S-HDL had no distinct effects on body weight, liver and spleen organ coefficients, and ALT, AST, and CK levels in xenografted mice, it could be concluded that encapsulating Sal into HDL significantly reduced its toxicity. Therefore, the aim of reducing toxicity and increasing the anti-ovarian cancer effects of Sal was realized by encapsulating it in HDL. However, more studies and data on long- and short-term toxicity are required to validate the safety of nanoparticles. We will consider this in our future research.

CSCs and EMT are promising areas currently being explored and can be targeted to eradicate ovarian cancer.<sup>27</sup> Abubaker et al found that residual OCCs in human OC xenografted mice, after chemotherapy treatment, were enriched with the CSCs phenotype, while ordinary OCCs, lacking the CSCs phenotype, were eliminated.<sup>35</sup> Silva et al found that

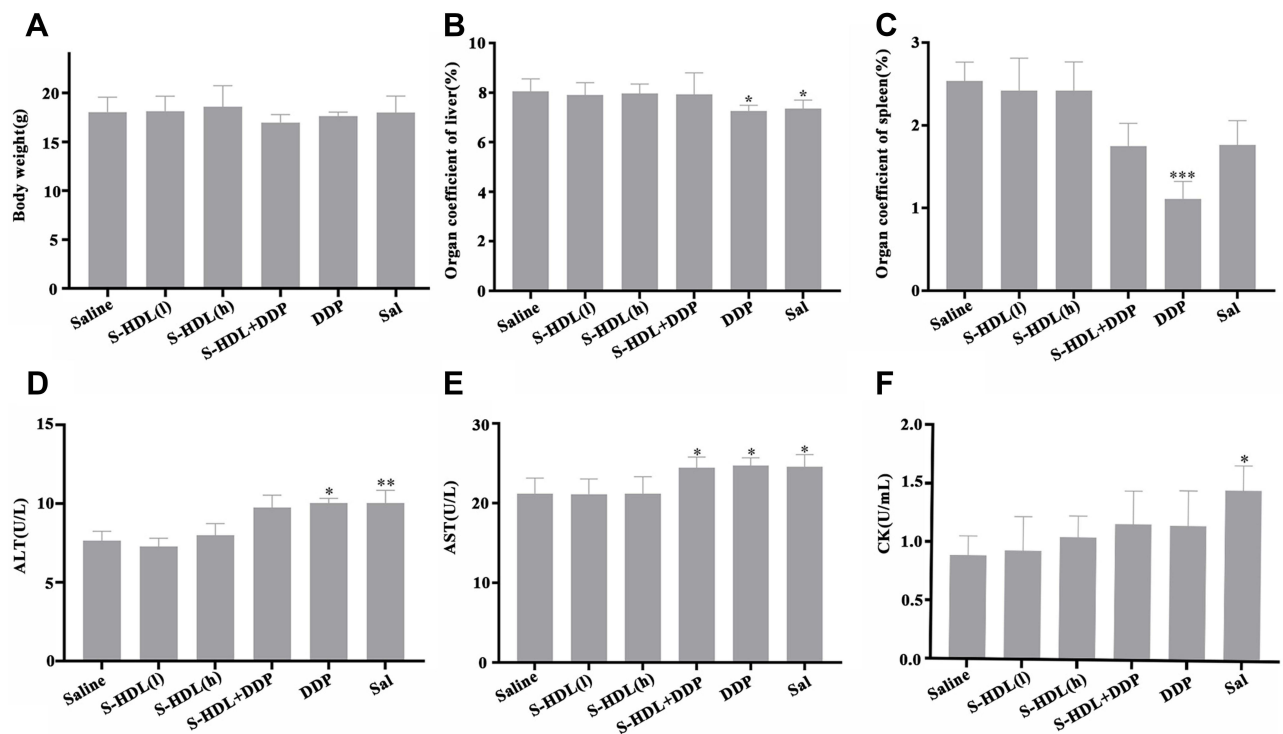


**Figure 7** Preliminary study on the safety of S-HDL. (A) Body mass of xenografted mice after being removed tumor, (B) organ coefficient of liver, (C) organ coefficient of spleen, (D) ALT level in serum, (E) AST level in serum and (F) CK level in serum of xenografted mice after treated with S-HDL for 3 weeks ( $\bar{x} \pm s$ , n=6) (\* $P < 0.05$ , \*\* $P < 0.01$ , \*\*\* $P < 0.001$ , #compared with saline treatment group).

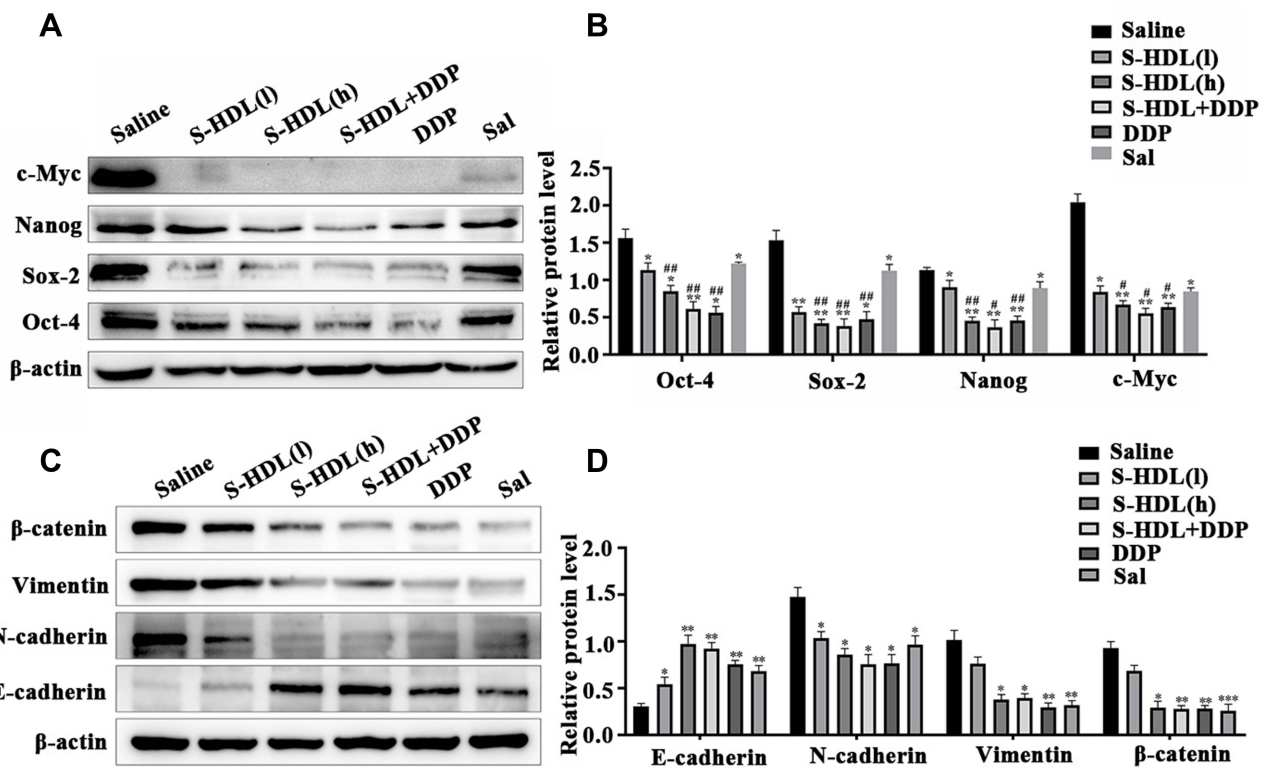


**Figure 8** S-HDL blocked stemness and EMT of ovarian cancer cells in xenografted mice. (A) Western blotting analysis results of c-Myc, Nanog, Oct-4 and Sox-2. (B) The statistical value of relative protein level. (C) Western blotting analysis results of E-cadherin, vimentin, N-cadherin and  $\beta$ -catenin. (D) The statistical value of relative protein level ( $\bar{x} \pm s$ , n=3) (\* $P < 0.05$ , \*\* $P < 0.01$ , \*\*\* $P < 0.001$ , #compared with saline treatment group, # $P < 0.05$ , ## $P < 0.01$ , ### $P < 0.001$ , \*compared with Sal treatment group).

ALDH<sup>+</sup> CD133<sup>+</sup> OCSCs, isolated from primary human ovarian tumors, showed greater chemotherapy resistance compared with parental cells, as well as reduced overall survival of OC patients.<sup>36</sup> EMT plays an important role in cancer invasion and metastasis to distant tissues, and in the development of resistance to chemotherapy.<sup>37</sup> In the current study, S-HDL inhibited the translation of stemness-related proteins (c-Myc, Nanog, Oct-4, and Sox-2) and suppressed EMT by upregulating E-cadherin and suppressing the translation of vimentin, N-cadherin, and  $\beta$ -catenin. Therefore, S-HDL may prevent recurrence and metastasis of ovarian cancer.

## Conclusion

The HDL delivery system significantly enhanced the uptake of encapsulated Sal by OCCs. Conversely, S-HDL could exert anti-ovarian cancer effects by inhibiting the proliferation of OCCs and OCSCs, promoting apoptosis, blocking EMT, and suppressing stemness and angiogenesis-related protein expression in vitro and in vivo. The anti-ovarian cancer effects of S-HDL were stronger than those of the unencapsulated Sal.

## Acknowledgments

We appreciate the assistance of Jilin Zhongke Bio-engineering Joint Stock Co., Ltd. and Jilin Prochance Biomedical Co., Ltd. for genome-wide analysis.

## Funding

This work was supported by the Science and Technology Department of Jilin Province (grant number 20210204148YY).

## Disclosure

The authors have declared that no competing interest exists.

## References

1. Stewart C, Ralyea C, Lockwood S. Ovarian cancer: an integrated review. *Semin Oncol Nurs*. 2019;35(2):151–156. doi:10.1016/j.soncn.2019.02.001
2. Torre L, Trabert B, DeSantis C, et al. Ovarian cancer statistics, 2018. *CA*. 2018;68(4):284–296. doi:10.3322/caac.21456
3. Sato R, Semba T, Saya H, Arima Y. Concise review: stem cells and epithelial-mesenchymal transition in cancer: biological implications and therapeutic targets. *Stem Cells*. 2016;34(8):1997–2007. doi:10.1002/stem.2406
4. Steinbichler TB, Dudas J, Skvortsov S, Ganswindt U, Riechelmann H, Skvortsova II. Therapy resistance mediated by cancer stem cells. *Semin Cancer Biol*. 2018;53:156–167. doi:10.1016/j.semcancer.2018.11.006
5. Visvader JE, Lindeman GJ. Cancer stem cells in solid tumours: accumulating evidence and unresolved questions. *Nat Rev Cancer*. 2008;8(10):755–768. doi:10.1038/nrc2499
6. Zhao Y, Dong Q, Li J, et al. Targeting cancer stem cells and their niche: perspectives for future therapeutic targets and strategies. *Semin Cancer Biol*. 2018;53:139–155. doi:10.1016/j.semcancer.2018.08.002
7. Lamouille S, Xu J, Derynck R. Molecular mechanisms of epithelial-mesenchymal transition. *Nat Rev Mol Cell Biol*. 2014;15(3):178–196. doi:10.1038/nrm3758
8. Nieto MA, Huang RY, Jackson RA, Thiery JP. EMT: 2016. *Cell*. 2016;166(1):21–45. doi:10.1016/j.cell.2016.06.028
9. Naujokat C, Fuchs D, Opelz GJ. Salinomycin in cancer: a new mission for an old agent. *Molecular Medicine Reports*. 2010;3(4):555–559. doi:10.3892/mmr\_00000296
10. An H, Kim JY, Lee N, Cho Y, Oh E, Seo JH. Salinomycin possesses anti-tumor activity and inhibits breast cancer stem-like cells via an apoptosis-independent pathway. *Biochem Biophys Res Commun*. 2015;466(4):696–703. doi:10.1016/j.bbrc.2015.09.108
11. Lee HG, Shin SJ, Chung HW, et al. Salinomycin reduces stemness and induces apoptosis on human ovarian cancer stem cell. *J Gynecol Oncol*. 2017;28(2):e14. doi:10.3802/jgo.2017.28.e14
12. Mao J, Fan S, Ma W, et al. Roles of Wnt/ $\beta$ -catenin signaling in the gastric cancer stem cells proliferation and salinomycin treatment. *Cell Death Dis*. 2014;5:e1039. doi:10.1038/cddis.2013.515
13. Tang QL, Zhao ZQ, Li JC, et al. Salinomycin inhibits osteosarcoma by targeting its tumor stem cells. *Cancer Lett*. 2011;311(1):113–121. doi:10.1016/j.canlet.2011.07.016
14. Li T, Su L, Zhong N, et al. Salinomycin induces cell death with autophagy through activation of endoplasmic reticulum stress in human cancer cells. *Autophagy*. 2013;9(7):1057–1068. doi:10.4161/auto.24632
15. Endo S, Nakata K, Sagara A, et al. Autophagy inhibition enhances antiproliferative effect of salinomycin in pancreatic cancer cells. *Pancreatol*. 2017;17(6):990–996. doi:10.1016/j.pan.2017.08.009
16. Kim KY, Park KI, Kim SH, et al. Salinomycin induces reactive oxygen species and apoptosis in aggressive breast cancer cells as mediated with regulation of autophagy. *Anticancer Res*. 2017;37(4):1747–1758.
17. Markowska A, Sajdak S, Markowska J, Huczynski A. Angiogenesis and cancer stem cells: new perspectives on therapy of ovarian cancer. *Eur J Med Chem*. 2017;142:87–94. doi:10.1016/j.ejmech.2017.06.030

18. Klose J, Eissele J, Volz C, et al. Salinomycin inhibits metastatic colorectal cancer growth and interferes with Wnt/beta-catenin signaling in CD133 (+) human colorectal cancer cells. *BMC Cancer*. 2016;16(1):896. doi:10.1186/s12885-016-2879-8
19. Yu Z, Cheng H, Zhu H, et al. Salinomycin enhances doxorubicin sensitivity through reversing the epithelial-mesenchymal transition of cholangiocarcinoma cells by regulating ARK5. *Braz J Med Biol Res*. 2017;50(10):e6147. doi:10.1590/1414-431x20176147
20. Awad L. Synthesis of chemical tools to improve water solubility and promote the delivery of salinomycin to cancer cells. *Exp Ther Med*. 2020;19(3):1835–1843. doi:10.3892/etm.2019.8368
21. Zhao P, Dong S, Bhattacharyya J, Chen M. iTEP nanoparticle-delivered salinomycin displays an enhanced toxicity to cancer stem cells in orthotopic breast tumors. *Mol Pharm*. 2014;11(8):2703–2712. doi:10.1021/mp5002312
22. Chen J, Ding J, Xu W, et al. Receptor and microenvironment dual-recognizable nanogel for targeted chemotherapy of highly metastatic malignancy. *Nano Letters*. 2017;17(7):4526–4533. doi:10.1021/acs.nanolett.7b02129
23. Vanags LZ, Wong NKP, Nicholls SJ, Bursill CA. High-density lipoproteins and Apolipoprotein A-I improve stent biocompatibility. *Arterioscler Thromb Vasc Biol*. 2018;38(8):1691–1701. doi:10.1161/ATVBAHA.118.310788
24. Strickland D, Ashcom J, Williams S, Burgess W, Migliorini M, Argraves W. Sequence identity between the alpha 2-macroglobulin receptor and low density lipoprotein receptor-related protein suggests that this molecule is a multifunctional receptor. *J Biol Chem*. 1990;265(29):17401–17404.
25. Yin X, Lu Y, Zou M, et al. Synthesis and characterization of salinomycin-loaded high-density lipoprotein and its effects on cervical cancer cells and cervical cancer stem cells. *Int J Nanomed*. 2021;16:6367–6382. doi:10.2147/IJN.S326089
26. Skubitz AP, Taras EP, Boylan KL, et al. Targeting CD133 in an in vivo ovarian cancer model reduces ovarian cancer progression. *Gynecol Oncol*. 2013;130(3):579–587. doi:10.1016/j.ygyno.2013.05.027
27. Ghahhari NM, Babashah S. Interplay between microRNAs and WNT/beta-catenin signalling pathway regulates epithelial-mesenchymal transition in cancer. *Eur J Cancer*. 2015;51(12):1638–1649. doi:10.1016/j.ejca.2015.04.021
28. Lutgendorf S, Penedo F, Goodheart M, et al. Epithelial-mesenchymal transition polarization in ovarian carcinomas from patients with high social isolation. *Cancer*. 2020;126(19):4407–4413. doi:10.1002/cncr.33060
29. Thiery C. Epithelial-mesenchymal transitions in tumour progression. *Nat Rev Cancer*. 2002;2(6):442–454.
30. Paredes F, Williams HC, San Martin A. Metabolic adaptation in hypoxia and cancer. *Cancer Lett*. 2021;502:133–142. doi:10.1016/j.canlet.2020.12.020
31. Cao Y, Arbiser J, D'Amato R, et al. Forty-year journey of angiogenesis translational research. *Sci Transl Med*. 2011;3(114):114rv113.
32. Baldwin H, Shen H, Yan H, et al. Platelet endothelial cell adhesion molecule-1 (PECAM-1/CD31): alternatively spliced, functionally distinct isoforms expressed during mammalian cardiovascular development. *Development*. 1994;120(9):2539–2553. doi:10.1242/dev.120.9.2539
33. Le C, Bennisroune A, Collin G, et al. LRP-1 promotes colon cancer cell proliferation in 3D collagen matrices by mediating DDR1 endocytosis. *Front Cell Develop Biol*. 2020;8:412. doi:10.3389/fcell.2020.00412
34. Zhang Z, Cao W, Jin H, et al. Biomimetic nanocarrier for direct cytosolic drug delivery. *Angew Chem Int Ed Engl*. 2009;48(48):9171–9175. doi:10.1002/anie.200903112
35. Abubaker K, Luwor R, Escalona R, et al. Targeted disruption of the JAK2/STAT3 pathway in combination with systemic administration of paclitaxel inhibits the priming of ovarian cancer stem cells leading to a reduced tumor burden. *Front Oncol*. 2014;4:75. doi:10.3389/fonc.2014.00075
36. Silva I, Bai S, McLean K, et al. Aldehyde dehydrogenase in combination with CD133 defines angiogenic ovarian cancer stem cells that portend poor patient survival. *Cancer Res*. 2011;71(11):3991–4001. doi:10.1158/0008-5472.CAN-10-3175
37. Chen D, Wang J, Zhang Y, et al. Effect of down-regulated transcriptional repressor ZEB1 on the epithelial-mesenchymal transition of ovarian cancer cells. *Int J Gynecol Cancer*. 2013;23(8):1357–1366. doi:10.1097/IGC.0b013e3182a5e760

International Journal of Nanomedicine

Dovepress

## Publish your work in this journal

The International Journal of Nanomedicine is an international, peer-reviewed journal focusing on the application of nanotechnology in diagnostics, therapeutics, and drug delivery systems throughout the biomedical field. This journal is indexed on PubMed Central, MedLine, CAS, SciSearch®, Current Contents®/Clinical Medicine, Journal Citation Reports/Science Edition, EMBase, Scopus and the Elsevier Bibliographic databases. The manuscript management system is completely online and includes a very quick and fair peer-review system, which is all easy to use. Visit <http://www.dovepress.com/testimonials.php> to read real quotes from published authors.

Submit your manuscript here: <https://www.dovepress.com/international-journal-of-nanomedicine-journal>